Spatial Overlap of ON and OFF Subregions and Its Relation to Response Modulation Ratio in Macaque Primary Visual Cortex

Mario L. Mata and Dario L. Ringach

J Neurophysiol 93:919-928, 2005. First published Sep 15, 2004; doi:10.1152/jn.00668.2004

Journal of Neurophysiology publishes original articles on the function of the nervous system. It is published 12 times a year (monthly) by the American Physiological Society, 9650 Rockville Pike, Bethesda MD 20814-3991. ISSN: 0022-3077, ESSN: 1522-1598. Visit our website at http://www.the-aps.org/.

J Neurophysiol 93: 919–928, 2005.
First published September 15, 2004; doi:10.1152/jn.00668.2004.

Spatial Overlap of ON and OFF Subregions and Its Relation to Response Modulation Ratio in Macaque Primary Visual Cortex

Mario L. Mata[1] and Dario L. Ringach[2]

[1]*Department of Neurobiology, David Geffen School of Medicine; and* [2]*Departments of Neurobiology and Psychology, Biomedical Engineering Interdepartmental Program, Brain Research Institute, Jules Stein Eye Institute, David Geffen School of Medicine, University of California, Los Angeles, California*

Submitted 2 July 2004; accepted in final form 8 September 2004

Mata, Mario L. and Dario L. Ringach. Spatial overlap of ON and OFF subregions and its relation to response modulation ratio in macaque primary visual cortex. *J Neurophysiol* 93: 919–928, 2005. First published September 15, 2004; doi:10.1152/jn.00668.2004. We studied the spatial overlap of ON and OFF subregions in macaque primary visual cortex and its relation to the response modulation ratio (the F_1/F_0 ratio). Spatial maps of ON and OFF subregions were obtained by reverse correlation with a dynamic noise pattern of bright and dark spots. Two spatial maps, ON and OFF, were produced by cross-correlating the spike train with the location of bright and dark spots in the stimulus respectively. Several measures were used to assess the degree of overlap between subregions. In a subset of neurons, we also computed the F_1/F_0 ratio in response to drifting sinusoidal gratings. Significant correlations were found among all the overlap measures and the F_1/F_0 ratio. Most overlap indices considered, and the F_1/F_0 measure, had bimodal distributions. In contrast, the distance between on and off subregions normalized by their size was unimodal. Surprisingly, a simple model that additively combines ON and OFF subregions with spatial separations drawn from a unimodal distribution, can readily explain the data. These analyses clarify the relationship between subregion overlap and the F_1/F_0 ratio in macaque primary visual cortex, and a simple model provides a parsimonious explanation for the co-existence of bimodal distributions of overlap indices and a unimodal distribution of the normalized distance.

INTRODUCTION

Hubel and Wiesel (1962, 1968) defined simple and complex cells in primary visual cortex based, in part, on the spatial segregation between ON and OFF subregions assessed in hand-mapped receptive fields. A more quantitative classification technique was later introduced based on the ratio between the amplitude of the first harmonic and the mean of the response—the F_1/F_0 ratio—when cells are stimulated with drifting sinusoidal gratings (De Valois et al. 1982; Maffei and Fiorentini 1973; Movshon et al. 1978b; Skottun et al. 1991). The distribution of F_1/F_0 in primary visual cortex is bimodal, a finding that has been considered proof of the existence of discrete cell classes (Skottun et al. 1991). However, it has been proposed (Mechler and Ringach 2002) and recently confirmed (Priebe et al. 2004) that the bimodality of F_1/F_0 arises due to the spike threshold nonlinearity in an otherwise unimodal population of cells.

These findings weaken the idea that primary visual cortex is populated by discrete populations of simple and complex cells (Mechler and Ringach 2002; but see (Abbott and Chance 2002) for a different viewpoint). It could be argued, however, that the F_1/F_0 ratio does not represent a direct measure of the overlap between subregions. This is a valid concern because recent data seem to indicate that the F_1/F_0 ratio does not correlate well with subregion overlap in the primary visual cortex of awake animals (Kagan et al. 2003). Perhaps, as proposed originally, discrete cell classes are best revealed by direct measurement of the spatial separation between ON and OFF subregions (Dean and Tolhurst 1983; Heggelund 1986a; Hubel and Wiesel 1962, 1968; Kagan et al. 2003; Maske et al. 1985; Schiller et al. 1976a,b). Our aim in this study was to address this issue and, in doing so, to gain a better understanding of the spatial arrangement between ON and OFF maps and their relation to the F_1/F_0 ratio.

METHODS

Acute experiments were performed on adult Old World monkeys (*Macaca fascicularis*) weighing between 2.5 and 3.2 kg. The methods of preparation and single-cell recording are the same as those described elsewhere (Ringach et al. 2002a). Briefly, animals were tranquilized with intramuscular acepromazine (50 μg/kg) then anesthetized with intramuscular ketamine (30 mg/kg) and maintained on intravenous opioid anesthetic (sufentanil citrate, 6 $\mu g \cdot kg^{-1} \cdot h^{-1}$) for the surgery. For recording, anesthesia was continued with sufentanil (6 $\mu g \cdot kg^{-1} \cdot h^{-1}$) and paralysis induced with pancuronium bromide (0.1–0.2 $mg \cdot kg^{-1} \cdot h^{-1}$). Electrocardiogram, electroencephalogram (EEG), and end-tidal CO_2 were continuously monitored. Blood pressure was measured noninvasively at 5-min intervals. Body temperature was maintained near 37°C via a heating blanket. All procedures have been approved by the UCLA Animal Research Committee and follow U.S. Department of Agriculture regulations and the National Institutes of Health Guideline for the Care and Use of Laboratory Animals.

We recorded from $n = 300$ cells in macaque V1. $n = 146$ neurons were recorded using a system of four independently movable electrodes (Alpha-Omega, Nazareth, Israel), arranged at the corners of a 800-μm square. The rest of the dataset was obtained using 10×10 electrode arrays (Bionic Systems LLC, Salt Lake City, UT), with grid separation of 400 μm and electrode lengths of 1.0 and 1.5 mm. Electrical signals were amplified and sampled by a Bionic Technologies Cerebus system. The resulting data were transferred via a fiber optic to a computer that performed spike sorting in real time. Spikes were labeled with their time of arrival (relative to the beginning of the stimulus) with 1-ms accuracy. Single spikes were sorted off-line using custom software displaying the projection of the spike waveforms on the first three principal components axes. A Photo Research Model

Address for reprint requests and other correspondence: D. Ringach, Dept of Psychology, Franz Hall, Rm 7613, University of California, Los Angeles, CA 90095-1563 (E-mail: dario@ucla.edu).

The costs of publication of this article were defrayed in part by the payment of page charges. The article must therefore be hereby marked "*advertisement*" in accordance with 18 U.S.C. Section 1734 solely to indicate this fact.

703-PC spectro-radiometer was used to calibrate the display. Fixation rings made from titanium (Duckworth and Kent, UK) were employed to stabilize the globe of the eye and minimize eye movements. An ophthalmic antibiotic, and steroid combination (TobraDex, Alcon) was employed to prevent an inflammatory response to the fixation rings. Eyes were protected with (neutral) gas permeable contact lenses that were cleaned regularly. Initially, the eyes were refracted by direct ophthalmoscopy to bring the retinal image into focus for a stimulus one meter away from the eyes. Once neural responses were isolated, we measured spatial frequency tuning curves for the dominant eye and maximized the response at high spatial frequencies. This procedure was performed independently for both eyes. In all experiments stimulation was monocular through the dominant eye (the other eye was occluded). The eccentricity of the measured receptive fields ranged between 1 and 8°. At the conclusion of the acute experiments, the animal was killed with an overdose of pentothal sodium (60–100 μg/kg) in accordance with AVMA guidelines.

Stimulus display and calculation of the ON and OFF maps

The stimulus consisted of a sequence of small bright and dark "dots" flashed over the receptive field of the neuron. The dots had a contrast of 99% and were presented on top of a mean background of 56 cd/m^2. To maximize spatial resolution, the radii of the dots were chosen to be as small as possible while still generating a measurable map. We normally started with a radius equal to one-fifth the period of the optimal grating and adjusted accordingly. In some cases, when recording from a population of cells, we employed a fixed radius of 0.1° that proved adequate when recording at 1–8° eccentricity. Each dot was presented for 20 ms (2 frames at 100-Hz refresh rate) and then repositioned at random in a different location. The density of the dots ranged from 1 to 10 dots/°^{2}, and on average it was 6 dots/°^{2}. Receptive field sizes at the eccentricities we recorded from were on average 0.6×0.6°^{2}. Thus in any one stimulus frame, we had an average of 2.2 dots within the classical receptive field. The linear size of the stimulus patch was large enough to cover the receptive fields being recorded, and it ranged from 0.7 to 3°. The numbers of bright and dark dots on each frame were the same, so there were no variations in average luminance. The total experimental time was between 15 and 30 min. Neurons responded to the stimulus with mean spike rates ranging from 2 to 60 spikes/s. A few cells that were very directional selective did not respond at all to the stimulus and could not be studied.

Given a fixed time lag, τ, we separately calculated the cross-correlation between the neural response and the location of bright and dark dots τ ms before the spikes (Jones and Palmer 1987). The resulting spatial maps, computed on a pixel-size resolution, were smoothed with a Gaussian kernel with a SD equal to the radius of the dots. Next, we computed the variance of the maps at each time lag. We defined the optimal delay time as the time at which the map that achieved the largest variance peaked. The maps at the optimal delay time were then normalized by subtracting the baseline corresponding to the mean value of locations in the map away from the receptive field (obtained from the boundary of the stimulus), and dividing by the SD of the noise estimated by randomly shuffling the trials and responses. The resulting (z-scored) maps are denoted by h_{ON} and h_{OFF} (our findings, however, do not depend on this normalization, as nearly identical results were obtained when the raw maps were analyzed instead). The maps may contain both positive and negative values. *Positive* regions in the h_{ON} map (shown by red hues in Figs. 2 and 4) indicate a location in the receptive field where flashing a bright dot induced the cell to *increase* its firing rate above its mean. *Negative* regions in the h_{ON} map (shown by blue hues in Figs. 2 and 4) indicate locations in the receptive field where flashing a bright dot induced the cell to *reduce* its firing rate below its mean. A similar description applies to h_{OFF}. We define the ON subregion by the locations where a bright dot induce the cell to increase its firing rate (where h_{ON} is significantly higher than zero by requiring $h_{ON} > 3$). To select the dominant subregion, we only took the largest connected component of the binary image $h_{ON} > 3$. The largest connected component of a binary image is the largest set of connected pixels with a logical value of "1" (Haralick and Shapiro 1992). Two pixels were considered connected if they were next to each other horizontally or vertically (also called a 4-neighborhood). Similarly, the dominant OFF subregion was computed as the largest connected component of the locations where a dark dot induced the cell to increase its firing rate, $h_{OFF} > 3$. The area of a subregion is defined as the area of the pixels contained in the largest connected component. If only one subregion exists, we say the cell is "monocontrast," as it responds by increasing its firing rate only to one particular sign of contrast (Kagan et al. 2003). We also defined a region of interest, intended to represent locations in the maps with a large signal to noise, by finding those pixels where either $|h_{ON}| > 3$ or $|h_{OFF}| > 3$. As described in the following text, the computation of the overlap measures was performed using the map values restricted to this region of interest.

Analysis of the spatial relationship between h_{ON} and h_{OFF}

We computed five different measures to analyze the spatial relationship between h_{ON} and h_{OFF}. First, we computed a measure of *discreteness* as used by Dean and Tolhurst (1983) in cat area 17. We denote this measure by α, which is defined mathematically by

$$\alpha = \frac{\Sigma\,|h_{ON} - h_{OFF}|}{\Sigma\,|h_{ON}| + \Sigma|h_{OFF}|}$$

For a complex cell, one expects the cell's response to be independent of contrast polarity, in which case $h_{ON} \approx h_{OFF}$, making $\alpha \approx 0$. A simple cell would show antagonistic responses to bright and dark bars, meaning that $h_{ON} \approx -h_{OFF}$ (Ferster 1988; Hirsch 2003; Hirsch et al. 2002; Palmer and Davis 1981). In this case, the measure α is expected to be near one. The summation above is restricted to the region of interest.

Second, we computed the *correlation coefficient* between h_{ON} and h_{OFF}. We consider the spatial maps as vectors, and denote by $\|h\| = \sqrt{\langle h,h\rangle}$ the norm of the vector h and by $\langle h_{ON},h_{OFF}\rangle$ the inner product between two vectors. Then, the correlation coefficient can be written as

$$\rho = \frac{\langle h_{ON},h_{OFF}\rangle}{\|h_{ON}\|\,\|h_{OFF}\|}$$

which equals the cosine of the angle between the two vectors. In complex cells h_{ON} and h_{OFF} have similar shapes, and we expect $\rho \approx +1$. A simple cell would show antagonistic responses to bright and dark bars resulting in a value $\rho \approx -1$. The calculation is again restricted to the region of interest (including pixels with "noise" in this calculation rapidly biases the correlation coefficient to 0.)

Third, we computed the *normalized distance* as the ratio between the separation between the center of mass of the ON and OFF subregions and the mean square root of their areas

$$\delta = \frac{\|\bar{h}_{ON} - \bar{h}_{OFF}\|}{\frac{1}{2}\left(\sqrt{A(h_{ON})} + \sqrt{A(h_{OFF})}\right)}$$

Here, $\bar{h}_{ON}$ is the center of mass of the ON subregion and $A(h_{ON})$ is its area, with similar definitions for h_{OFF}. $\|\bar{h}_{ON} - \bar{h}_{OFF}\|$ is the distance between the center of mass of the subregions. The idea is to measure the distance between the subregions normalized by their mean (linear) size. A complex cell is expected to have a small separation between the subregions relative to their size, resulting in values of $\delta \approx 0$. Simple cells are expected to have large separations between the subregions relative to their size, meaning $\delta \gg 0$. Monocontrast cells are excluded from this analysis, as they only have one significant subregion. An analysis was also done normalizing by the mean "width" of the subregions computed through a one-dimensional slice

of the maps (see following text). The resulting distribution was very similar and is not shown.

The next two measures were defined by first taking a one-dimensional slice through both maps. The slice was selected so that it passed through the center of mass of the ON subregion and the center of mass of the OFF subregion, as shown in the examples of Fig. 2. Monocontrast cells have to be necessarily excluded from these analyses. We define the slice through h_{ON} by g_{ON} and the slice through h_{OFF} by g_{OFF}. Given these one-dimensional spatial profiles we computed the following two additional measures.

Our fourth measure was obtained by fitting Gaussian functions to the profiles of g_{ON} and g_{OFF}, resulting in two different mean locations, m_{ON} and m_{OFF}, and SDs representing their widths, σ_{ON} and σ_{OFF}. Following the work of (Schiller et al. 1976c) we defined the *overlap index* by

$$\omega = \frac{(\sigma_{ON} + \sigma_{OFF}) - |m_{ON} - m_{OFF}|}{(\sigma_{ON} + \sigma_{OFF}) + |m_{ON} - m_{OFF}|}$$

For a complex cell where the separation is small relative to the width of the profiles, we expect $\omega \approx 1$, whereas for simple cells, we expect the separation to be large relative to the widths and $\omega < 0$. Again, monocontrast cells must be excluded from this analysis.

The fifth measure we considered was the *relative phase* measure defined by Conway and Livingstone (2003). The first step in the calculation involves the simultaneously fitting of sinusoidal functions of the form $A \sin(2\pi fx + \phi)$ to g_{ON} and g_{OFF}, where the spatial frequency is constrained to be the same for both maps. The relative phase measure is the difference between the fitted phases, $\Delta\phi = |\phi_{ON} - \phi_{OFF}|$ modulo 180°. If the peaks of g_{ON} and g_{OFF} occur in similar locations (as expected in complex cells), then one expects $\Delta\phi \approx 0°$. If the maps tend to be in anti-phase (simple cells), then $\Delta\phi \approx 180°$. In practice, to make the measure less sensitive to noise, the sinusoidal functions are windowed by a Gaussian and the center is constrained to be the same for both maps as well (see Conway and Livingstone 2003 for a discussion). We implemented their method in our calculations.

Measurement of the F_1/F_0 ratio

After measuring h_{ON} and h_{OFF}, the F_1/F_0 ratio was obtained in a subset of $n = 98$ neurons recording with 10×10 electrode arrays. We measured the response of the neurons to all combinations of 24 possible directions (15° spacing), and spatial frequencies ranging from 0.1 to 10 cycles/°, in 10 logarithmic steps. The temporal frequency was fixed at 3 Hz and the trial duration was 4 s. The stimulus was large enough to cover all the receptive fields in the array (usually $2 \times 2°$). For each cell, we used the orientation and spatial frequency that produced the maximal response to compute the F_1/F_0 ratio. Due the nature of the array experiments, the temporal frequency and the size of the stimuli were not optimized for each individual cell as we have done previously (Ringach et al. 2002b). In addition, the relatively coarse sampling of orientation and spatial frequency means that in some cases we might be slightly off the optimal value. The response at the optimal combination of orientation and spatial frequency was further required to be ≥10 spikes/s above the spontaneous rate (otherwise the data were not included.) The DC response, F_0, represents the elevation of the mean spike rate above the spontaneous firing of the cell measured during the presentation of "blank" trials where the screen had a uniform mean luminance value. A database containing the experimental values of the overlap indices and the F_1/F_0 ratio can be obtained from http://manuelita.psych.ucla.edu/~dario/neurodata.htm.

Descriptive model

We put forward a descriptive model of our data that assumes that the ON and OFF maps result from the linear combination of two subregions of opposite sign a distance d apart (Fig. 1), where d is distributed unimodally and generated by re-sampling the distribution of normalized distance in our data (Fig. 3; distribution of δ). Further, we assume that each subregion is organized in an antagonistic (push-pull) fashion. These two assumptions alone are sufficient to replicate the main features of our data set, including the bimodality of overlap measures and their correlations. Thus it is possible that a single mechanism could underlie the generation of the measured receptive fields.

To describe the model in more detail, let us denote the hypothetical (1-dimensional) map of the putative ON subunit obtained by cross-correlating the response with the location of bright dots by h^+_{ON} (red solid lines) and that obtained with dark dots by h^-_{ON} (red dashed lines) (Fig. 1*A*). The fact that they overlap in space but have opposite signature is a reflection of a push-pull organization. Similarly, we denote the hypothetical map of the OFF subunit obtained by correlating with the location of dark dots by h^+_{OFF} (blue solid lines) and its bright map by h^-_{OFF} (blue dashed lines). The kernels h^+_{ON} and h^+_{OFF} were selected to be two-dimensional Gaussians with unit variance and unit height (only their 1-dimensional profiles are shown in the Fig. 1). In each simulated receptive field, h^-_{ON} and h^-_{OFF} had the same shape as h^+_{ON} and h^-_{ON} but with a relative amplitude equal to -0.4. Thus the absolute magnitude of the "push" was larger than the absolute magnitude of the "pull."

We now assume that the receptive field of a cell is a linear combination of these maps with weights w^+ and w^- so that the resulting ON map for the cell is given by $h_{ON} = w^+h^+_{ON} + w^-h^-_{OFF}$, and

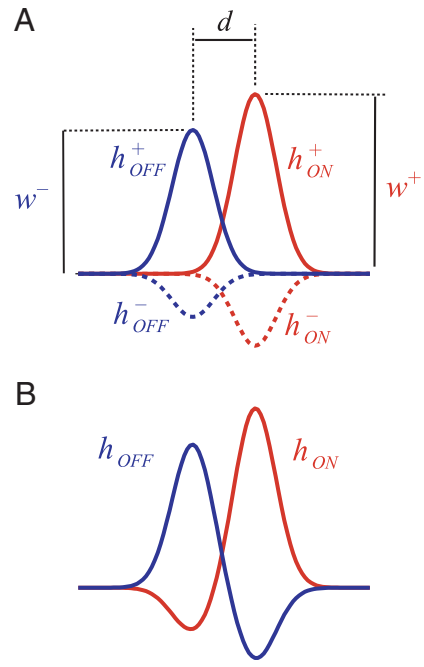

FIG. 1. A descriptive model. *A*: the model consists of the linear combination of 2 subunits, located a distance d apart, having a single subregion. Each subregion organized in a push-pull manner, meaning that stimuli of opposite contrast generate antagonistic responses. The hypothetical 1-dimensional slice of the ON subunit obtained with bright dots (h^+_{ON}) is shown by the solid red line, and its map obtained with dark dots (h^-_{ON}) is shown by the dashed red line. Similarly, the hypothetical profile of the OFF subunit obtained with dark dots (h^+_{OFF}) is shown by the solid blue curve, and its map obtained with bright dots (h^-_{OFF}) is shown by the dashed blue line. (*b*) The resulting maps for bright (h_{ON}, in red) and dark (h_{OFF}, in blue) stimuli after the linear combination of the subunits.

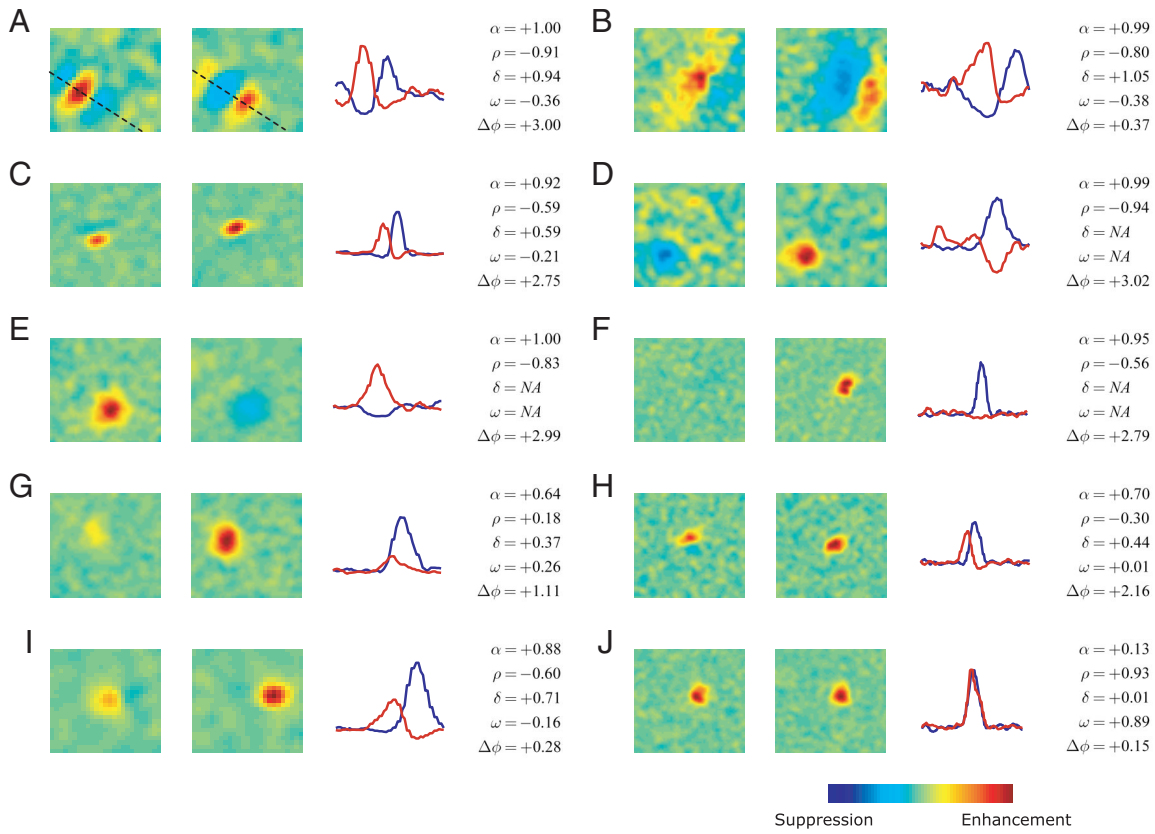

FIG. 2. ON and OFF maps in macaque V1. The figure depicts representative maps obtained via reverse correlation with sparse dot sequences. *Left*: each image represents the map corresponding to bright dots (h_{ON}); *middle*: image represents the map corresponding to dark dots (h_{OFF}). As indicated by the colormap (*bottom right*), regions in red represent areas where stimuli induced the cell to increase its firing rate above baseline; regions in blue show areas of the receptive field where stimuli of the corresponding contrast sign induced the cell to decrease its firing rate below baseline; while neutral areas appear in green. The curves on the right in each panel represent the one dimensional profile for the ON (red curve) and OFF (blue curve) maps. The 1-dimensional slices of the maps are defined to pass through the center of mass of the dominant subregions (see METHODS). The orientation of 1 such slice is shown as a dashed line in *A*. *Right*: the various overlap measures in each case.

the OFF map is $h_{OFF} = w^+ h^-_{OFF} + w^- h^-_{ON}$ (Fig. 1*B*). In other words, the ON map of the cell is a linear combination of the push provided by the ON subunit and the pull provided by the OFF subunit (with a similar description for the OFF map). The weights $w+$ and w^- were jointly normal (2.5 ± 1; mean $\pm$ SD). The weights were correlated with a coefficient of $+0.6$. Finally, additive white noise (0 ± 0.3) was added to the maps (see Fig. 4 for some examples of the simulated maps). This was done to generate simulated maps with signal-to-noise ratios comparable to the measured ones. The reason is that the computation of overlap measures involves the determination of a region of interest, and adding noise in the simulated maps ensures the data processing is identical for both cases. We have also verified that the results reported here do not depend strongly on the level of the noise.

RESULTS

We measured the spatiotemporal receptive fields of $n = 300$ cells in macaque primary visual cortex (area V1) using reverse correlation with a dynamic stimulus of bright and dark dots on top of a gray background (see METHODS). For each cell, two receptive field maps were obtained by cross-correlating the spike train of the neuron with the location of the bright dots (the ON map) or with the location of the dark dots (the OFF map) (Cai et al. 1997; Jones et al. 1987). The calculations were performed at time lags, t, ranging from 0 to 200 ms. The relationship between the maps was analyzed at the optimal time lag, defined as the point at which the map with the largest variance peaked (METHODS). We denote by h_{ON} the map obtained with bright dots and by h_{OFF} the map obtained with dark dots.

Examples of the measured maps in macaque primary visual cortex are illustrated in Fig. 2. In each case, we show h_{ON}, h_{OFF}, and a plot of the one-dimensional slices that pass through the center of mass of both subregions (see METHODS). The numeric measures listed to the right of the panels represent the value of the overlap indices in each case, and they will be discussed in detail in the following text. As expected from the classical definition of simple cells, we observed maps with two subregions and antagonistic responses to bright and dark stimuli (Fig. 2, *A–C*). The degree of antagonism varied, and it could be large (Fig. 2*A*) or small (Fig. 2*C*). We also observed cells that showed only one effective "subregion" with antagonistic responses (Fig. 2, *D–F*). Again, the degree of antagonism varied from large (Fig. 2*D*) to small (Fig. 2*F*). In some cases, the relationship between the maps was not so clear. Some cells appeared to have maps where there was antagonism in one of the subregions but not the other (Fig. 2, *H* and *I*). Finally, as expected from the classical description of complex cells, we observed cases where the responses to bright and dark stimuli overlapped strongly (Fig. 2, *G* and *J*). The degree to which the responses to bright and dark stimuli were of similar amplitude varied across the population. While in some cases the re-

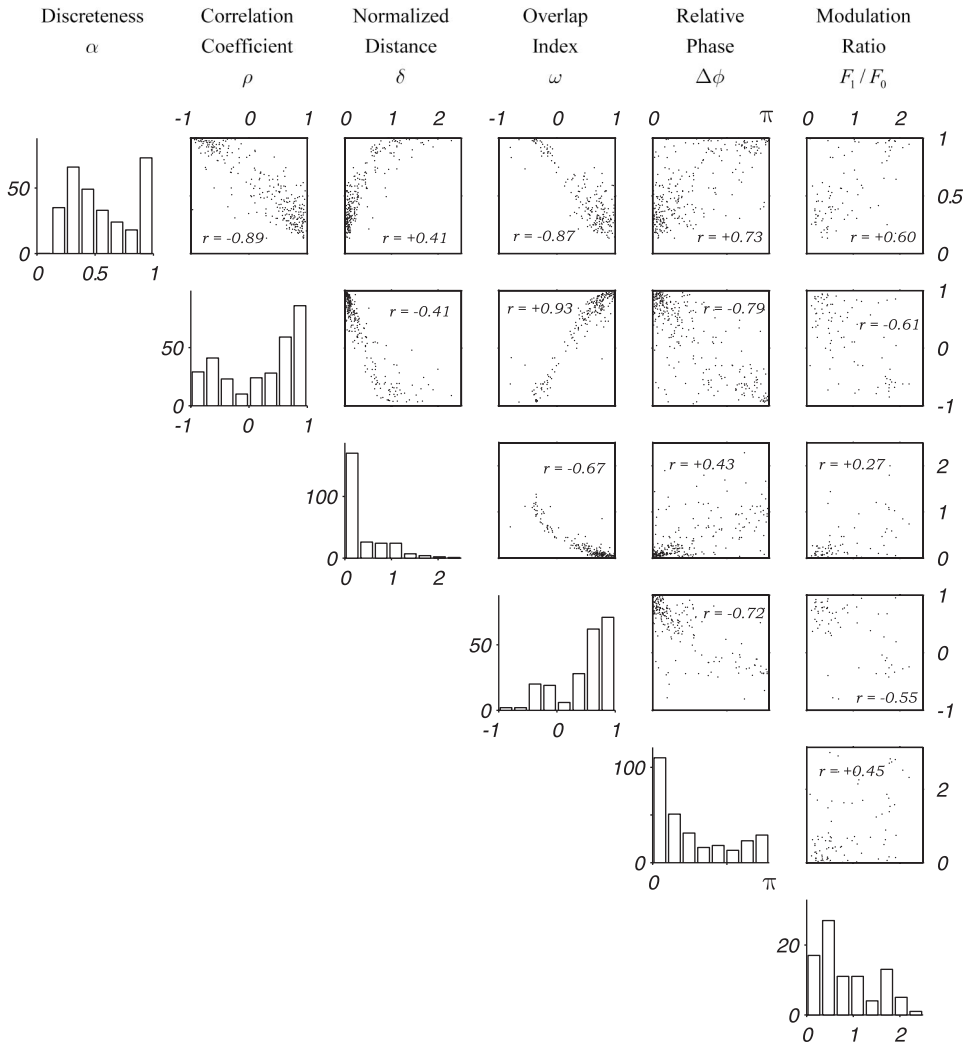

FIG. 3. Distribution of subregion overlap and modulation ratio in macaque primary visual cortex. On the main diagonal, from top left to bottom right, we show the histograms of the discreteness measure, the correlation coefficient, the normalized distance, the overlap index, the relative phase, and the modulation ratio. All the distributions except for the normalized distance show signs of bimodality. The scatter plot between each pair of variables is shown off the main diagonal. All measures are significantly correlated ($P < 0.01$). The correlation coefficient for each case appears at the *inset* to the scatter plots.

sponses were nearly equal (Fig. 2*J*), in others one of the contrasts was clearly dominant (Fig. 2*G*).

The distribution of our five measures of subregion overlap and the F_1/F_0 ratio in our V1 population is shown in the main diagonal of graphs in Fig. 3. The scatter plots among all these variables are plotted off the main diagonal. The distribution of Dean and Tolhurst's discreteness measure, α, and the correlation coefficient, ρ, are clearly bimodal (Hartigan's dip test, $P < 0.001$). The distributions of Schiller et al.'s overlap index, ω; Conway and Livingstone's relative phase, $\Delta\phi$; and the F_1/F_0

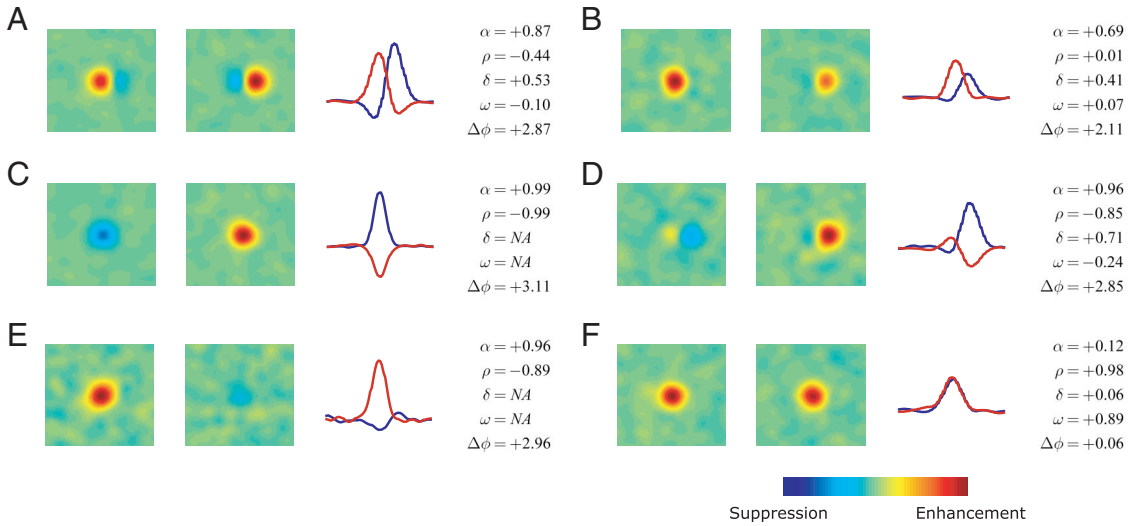

FIG. 4. Examples of maps generated by the model. The format is the same as that of Fig. 2. The model generates maps that resemble those observed experimentally.

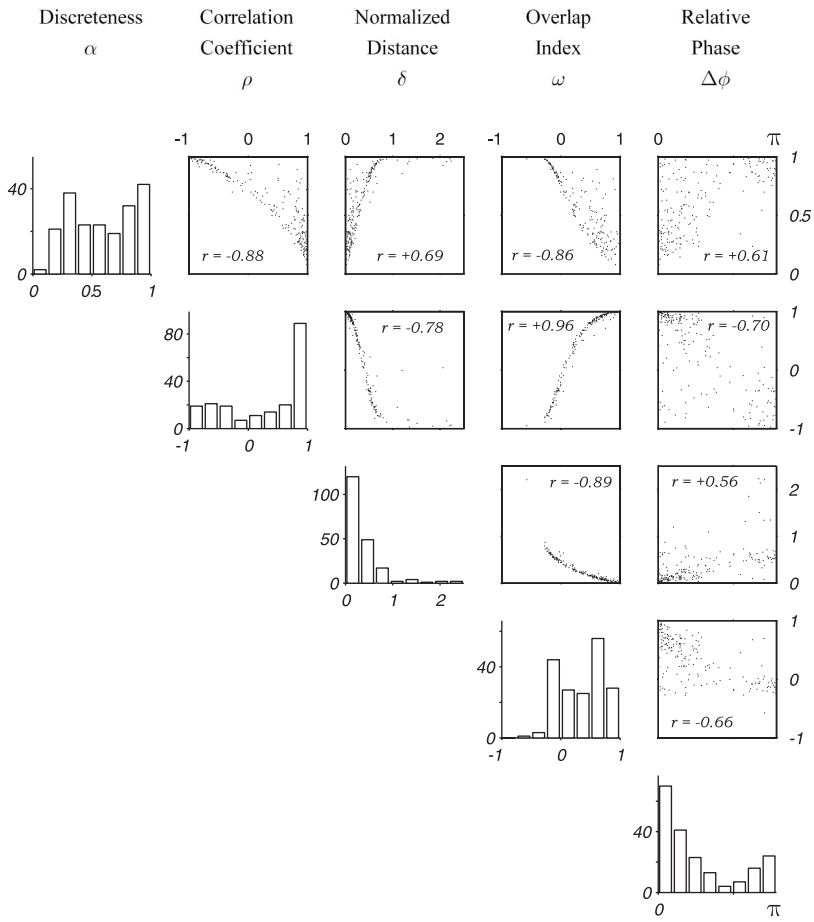

FIG. 5. Distribution of subregion overlap resulting from the simulation of $n = 250$ receptive fields by the model. On the main diagonal, from top left to bottom right, we show the histograms of the discreteness measure, the correlation coefficient, the normalized distance, the overlap index, and the relative phase. All the distributions except for the normalized distance show signs of bimodality. The scatter-plot between each pair of variables is shown off the main diagonal. All measures are significantly correlated ($P < 0.01$). The correlation coefficient for each case appears at the inset to the scatter plots. The results resemble quite well the main features of our data, including the bimodality of the various overlap measures and the unimodal nature of the normalized distance.

ratio show a trend towards bimodality (Hartigan's dip test, $P < 0.01$). The one measure that cannot be ruled out to be unimodal is the normalized distance, δ (Hartigan's dip test, $P = 0.99$).

The scatter plots between the overlap measures show that they tend to be well correlated (all correlation values are significant at the 0.01 level). The correlation values varied, ranging in *absolute* value from 0.41 (between δ and ρ) to 0.93 (between ω and ρ). The F_1/F_0 response modulation ratio was most correlated with the correlation coefficient measure ρ ($r = -0.61$), and least correlated with the normalized distance δ ($r = +0.27$). Interestingly, we find a reasonably good correlation between the overlap index ω and the F_1/F_0 ratio ($r = -0.55$), which contrasts with a recent report that finds no statistical correlation between these measures in awake monkeys (Kagan et al. 2003). All the signs of the correlation coefficients are as expected, meaning that simple cells in one measure tended to be simple cells in another measure and the same for complex cells.

Relationship between overlap and modulation ratio in a simple model

While some of the overlap measures show a bimodal distribution, the normalized distance, which is perhaps the most direct interpretation of the classic description of subregion overlap, is unimodal. In addition, all the measures studied showed a significant degree of correlation, suggesting that a single underlying mechanism could be sufficient to explain the structure of ON and OFF maps. In this section, we explore the possibility that a simple model could explain both the unimodal distribution of normalized distance and the bimodality of the various subregion overlap measures.

There are two key assumptions in the model. First, we assume that receptive fields are the result of the combination of ON and OFF subunits a distance *d* apart (Fig. 1*A*). Second, we assume that these subunits already show antagonistic responses to bright and dark stimuli (a push-pull arrangement). The distance between the subunits, *d,* was generated by re-sampling from the empirical distribution of the normalized distance (Fig. 3; distribution of δ).

Representative maps generated by the model, together with their respective one-dimensional profiles and the resulting measures of overlap are illustrated in Fig. 4. Receptive fields with well segregated ON and OFF subregions showing antagonistic responses to bright and dark stimuli are generated when the two units are weighted nearly equally and the separation *d* is large (Fig. 4*A*). Receptive fields with similar responses to bright and dark dots are generated when the two units are weighted nearly equally and the separation *d* is small (Fig. 4*F*). If only one subunit is dominant because it is weighted more strongly than the other, the result is a receptive field with only one subregion with push-pull organization (Fig. 4*C*). The model also generates intermediate cases resembling those in the experimental data (Fig. 4, *B, D,* and *E*).

The distribution of the five measures of subregion overlap in the model is shown in the main diagonal of graphs in Fig. 5. The scatter plots among all these variables are plotted off the

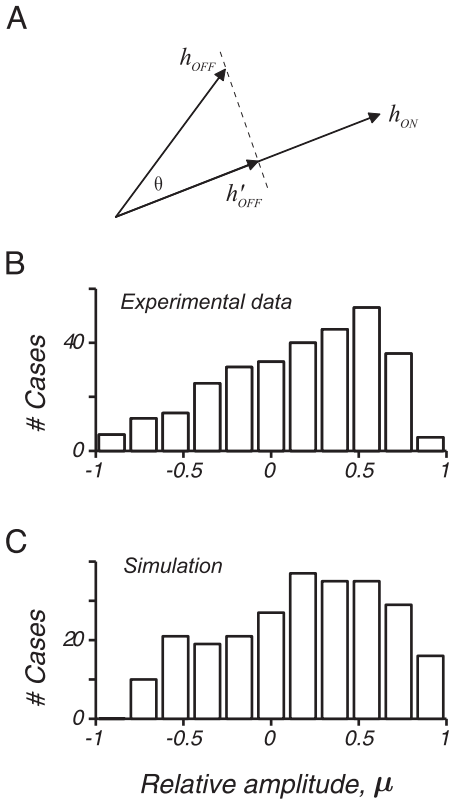

FIG. 6. The relative amplitude measure. *A*: the relative amplitude μ is the relative length of the smaller map projected onto the larger map. In this example, it would be the length of h_{OFF} divided by the length of h_{ON}. Complex cells are expected to yield $\mu \approx +1$, while simple cells are expected to yield $\mu \approx -1$. *B*: the distribution of relative amplitude in V1 is unimodal and is also well explained by the model, as shown in *C*.

main diagonal. The distribution of all the measures, except for the normalized distance, are statistically bimodal (Hartigan's dip test, $P < 0.05$). Furthermore, it can be seen that the joint distribution of the scatter plots replicates well the one observed experimentally. This demonstrates that a unimodal distribution of normalized distance and the bimodality of the overlap indices could potentially be generated by a simple mechanism. The model provides a reasonable explanation for the shape of the marginal distributions and their correlations.

Origin of bimodal distributions

The reason for the bimodality in the distributions can be traced back to a type of "nonlinear ruler" effect (Mechler and Ringach 2002). This means that under certain conditions, the measure changes its numeric value very rapidly when the maps are changed very little. We think such highly nonlinear behavior results from two main reasons. One is the fact that the relative magnitude of the maps is ignored by these measures. Another contributor to this effect, which occurs in experiments that measure the subregions using flashing or drifting bars in neurons with low spontaneous activity (Hubel and Wiesel 1962, 1968; Schiller et al. 1976b), is the thresholding involved in spike generation (Mechler and Ringach 2002; Priebe et al. 2004).

To appreciate how insensitivity to the magnitude of the maps contributes to the bimodality of the distributions consider the behavior of the correlation coefficient in the maps shown in Fig. 2, *F* and *G*. The two cells are dominated by an OFF subregion, and the response to bright dots was weak. The overlap between the two is significant in both cases; however, in one case, the ON map tends to be slightly negative (Fig. 2*F*) and in the other case, positive (Fig. 2*G*). It can readily be seen that a small change in sign in the weak response can have a large effect in the resulting correlation coefficient. The example in Fig. 2*F* has $\rho = -0.56$ (suggesting one should classify this cell as "simple") and the example in Fig. 2*G* has $\rho = 0.18$ (suggesting one should classify this cell as "complex"). In general, if we assume the two maps have identical shapes, $h_{ON} = h$ and $h_{OFF} = \epsilon h$, then $\rho = +1$ if $\epsilon > 0$, and $\rho = -1$ if $\epsilon < 0$, no matter how small ϵ is. This is because the correlation coefficient is insensitive to the *magnitude* of the maps and only measures the *similarity* between their shapes as the cosine of the angle between the vectors. Any measure that shows such nonlinear behavior with respect to small changes in the maps should be considered potentially problematic. It is easy to see that a similar behavior applies to the relative phase measure, as $\Delta\phi = 0°$ if $\epsilon > 0$ and $\Delta\phi = 180°$ if $\epsilon < 0$. Thus relative phase is also a very nonlinear function of the maps. The discreteness measure α is insensitive to the magnitude of the maps as long as they have different signs at each location. For example, even though the examples in Fig. 2, *D* and *F*, could be considered to be rather different map pairs, both cases achieve $\alpha \approx 1$ (suggesting both neurons should be classified as simple). If the maps tend to have the same sign, the resulting measure will be much lower even though one of the maps is weak. For comparison, the example of Fig. 2*G* has $\alpha = 0.64$. Finally, the overlap index proposed by Schiller et al. is insensitive to the magnitude of the maps as well. This is because only the distance between the ON and OFF subregions, and their widths, are used in the calculation of the overlap index. The amplitudes of the maps are ignored.

Measure sensitive to the magnitude of the maps

Prompted by the realization that the measures showing bimodal distributions are all insensitive to the relative magnitude of the maps, we decided to investigate a measurement that does take this factor into account. We define the *relative amplitude* as

$$\mu = \frac{\min(\|h_{ON}\|, \|h_{OFF}\|)}{\max(\|h_{ON}\|, \|h_{OFF}\|)} \cos\theta$$

where θ is the angle between the two maps. This measure has a straightforward geometric interpretation (Fig. 6*A*). It represents the relative amplitude of the map with the smaller norm after its projection onto the map with the larger norm. Complex cells, the response of which is invariant to contrast sign, are expected to yield values of μ close to $+1$. Simple cells (obeying perfect linearity) are expected to yield values of μ near -1. The distribution of relative amplitude in primary visual cortex is unimodal (Fig. 6*B*, Hartigan's dip test, $P > 0.9$), broad, and has a mean slightly above zero [0.15 ± 0.025 (mean $\pm$ SE)]. The distribution of relative overlap generated by the model is shown in Fig. 6*C*. The empirical and simulated distributions are not statistically different (Kolmogorov-Smirnov test, $P = 0.47$). Thus a measure that takes into account the relative amplitudes of the maps does not show any obvious sign for the presence of discrete neuronal populations.

The relative amplitude measure is not without pitfalls. One problem is that the amplitudes of the kernels might depend on the density of the dots (Simoncelli et al. 2004). If a small number of dots is present within the receptive field at any one time (sparse noise), it is possible that the measurements indicating "response enhancement" are overemphasized compared with those showing "response suppression." In other words, with sparse noise, an accelerating output nonlinearity involved in spike generation could distort the actual magnitudes of the maps. However, in a few cases, we have obtained maps at various levels of dot density and observed little change in the maps (data not shown). Thus it is possible that in practice this is not a serious problem, but more data are needed to carefully establish the dependence of map amplitude as a function of dot density. Recording the intracellular membrane potential instead of extracellular data may be one route to obtain more accurate estimates of the magnitudes (Hirsch 2003; Priebe et al. 2004). However, one must be aware that in such experiments the relative magnitudes of the push and pull will depend on the resting membrane potential the cell is being held to. Thus while there are certain complications in the measurement of the relative size of the push and pull, ignoring their magnitudes appears not to be an appropriate solution as it generates a family of measures with highly nonlinear behavior.

DISCUSSION

In a seminal paper, Dean and Tolhurst (1983) provided an early critique of the classification of simple and complex cells (see also the discussion in Henry 1977). They also showed, for the first time, that there was a good correlation between subregion overlap (the discreteness measure) and the F_1/F_0 ratio in cat primary visual cortex. Efforts by Spitzer and Hochstein showed that accounting for the shape of response histograms to drifting and contrast reversal gratings appeared to require more than two discrete classes of neurons, and that "intermediate" behavior could be observed in numerous situations (Spitzer and Hochstein 1988, 1985a,b). Some of these concerns subsided after the publication of Skottun et al. (1991), which demonstrated a consistent bimodal distribution of the F_1/F_0 ratio in both monkey and cat, using data from various laboratories. These investigators also showed that classifying neurons using the F_1/F_0, or by the classic method of manually mapping the neurons with flashing bars, agreed very well. The bimodal distribution of the F_1/F_0 ratio alone was considered sufficient to demonstrate the existence of distinct simple and complex cell populations. However, the recent proposal (Mechler and Ringach 2002) and its experimental verification (Priebe et al. 2004) that the bimodality of the F_1/F_0 ratio arises as a consequence of spike thresholding in an otherwise unimodal population of neurons has prompted a re-evaluation of the distinctness of simple and complex classes. One possibility is that, as proposed originally by Hubel and Wiesel, discrete cell classes are best revealed by the analysis of the spatial organization of ON and OFF subregions (Dean and Tolhurst 1983; Heggelund 1986a,b; Hubel and Wiesel 1962, 1968; Kagan et al. 2003; Maske et al. 1985; Schiller et al. 1976a–c). This possibility was the motivation behind the present study where we analyzed subregion overlap and the F_1/F_0 ratio in macaque V1 using modern mapping techniques.

Our findings indicate that, consistent with previous reports, some measures of subregion overlap are bimodal. These include the discreteness measure of Dean and Tolhurst (1983), the correlation coefficient (DeAngelis et al. 1999; Priebe et al. 2004), the relative phase measure (Conway and Livingstone 2003), and the overlap index (Kagan et al. 2003; Schiller et al.1976c). The modulation ratio also shows a tendency for bimodality as already established in previous studies (Ringach et al. 2002b; Skottun et al. 1991). In contrast to our previous study (Ringach et al. 2002b), the bimodality in the F_1/F_0 distribution of the present population failed to achieve statistical significance. This is most likely a consequence of the fact that we measured it under conditions that were not optimized for each individual cell (see METHODS) (Movshon et al. 1978a,b; Skottun et al. 1991). We also found that the distribution of the normalized distance between the ON and OFF subregions is unimodal. This was somewhat curious because the normalized distance is, arguably, the most direct implementation of the classic definition of subregion overlap. If simple and complex cells were distinct classes, one would expect to see a bimodal distribution of normalized distance, but we did not.

We demonstrated that a unimodal distribution of normalized distance and the bimodal distribution of various overlap measures can co-exist in a simple model where two subregions, one ON and one OFF, by themselves organized in a push-pull manner, are linearly combined. The model is admittedly too simplistic. Nevertheless, it does a good job at approximating the measured distributions and their correlations. The model resembles, to some extent, the haphazard connectivity model between the LGN and V1 (Ringach 2004), where simple cells in cat layer 4 are postulated to result from the statistical pooling of thalamic afferents. Perhaps, extending the haphazard connectivity model one more "layer," by having superficial layer neurons statistically pool from layer 4 neurons, may generate an entire population of receptive fields with maps similar to the ones we observed here. Nevertheless, in its present form, the model provides only a description of subregion overlap across the V1 population and should not be taken to imply a particular organization of the underlying circuitry. We note that more detailed computational models than the one considered here have already shown that simple and complex cells can arise as the ends of the spectrum in networks with nonspecific connectivity (Abbott and Chance 2002; Chance et al. 1999; Tao et al. 2004). In particular, Tao et al. (2004), have shown that a bimodal distribution of F_1/F_0 arises in a large-scale model of layer $4C\alpha$. It would be of interest to see if an analysis of subregion overlap and its relation to the F_1/F_0 ratio in these models can replicate aspects of our data.

We suggested that a likely reason for the bimodality of the overlap measures is their high degree of nonlinearity in some situations. This means that, under certain conditions, the measures generate very different values when the maps change very little. It was argued that the behavior is a partial consequence of these measures being insensitive to the magnitudes of the maps. A measure that takes this into account (the relative magnitude, μ) did not show any clear evidence of bimodality. Caution should be exercised in comparing the amplitude of the kernels (see DISCUSSION in the preceding text), but we believe the present analyses show that ignoring the amplitudes by normalizing them does not constitute a solution to the problem.

Finally, our results indicate that the various overlap measures and the response modulation ratio show significant correlations among themselves. This is in agreement with the quantitative data of Dean and Tolhurst (1983) and is also consistent with the agreement in the classification of cells using either the modulation ratio or manual mapping of the receptive fields (Skottun et al. 1991). Such results would not be expected if the F_1/F_0 ratio did not correlate with the overlap between subregions. Our data disagree with a recent report (Kagan et al. 2003) that modulation ratio and subregion overlap are not significantly correlated in primary visual cortex of awake monkeys. At present, we do not have a good explanation for this discrepancy except to state that our preparations are different (our study was done in the anesthetized animal) and our methods to map the receptive fields differ (we used a reverse correlation technique, while Kagan et al. (2003) employed drifting bars).

Despite the long-held belief that there are two discrete neuronal classes in V1, the null hypothesis should be that of a continuum of receptive field attributes. We believe our data and the accompanying analysis, together with similar findings in cat area 17 (Priebe et al. 2004), show that neither the F_1/F_0 ratio nor subregion overlap convincingly demonstrate the existence of discrete classes of simple and complex cells in primary visual cortex. Of course, one cannot "prove" that there is a continuum between simple and complex cells (the null hypothesis). There is always the possibility that future studies will reveal a clear segregation into neuronal classes based on measurement(s) not considered here.

The original description of discrete classes of simple and complex cells and the associated hierarchical model proposed by Hubel and Wiesel have had a strong impact in shaping theories of V1 function. Influenced by the classic framework, many investigators have developed theories of how simple cells represent the visual image, deferring the question about the function of complex cells, the logic being that in a strict hierarchy we can study cortical function one level at a time (Bell and Sejnowski 1997; De Valois et al. 1979; Hurri and Hyvarinen 2003; Kulikowski and Bishop 1981; Maffei and Fiorentini 1973; Olshausen 2002; Olshausen and Field 1996; Simoncelli and Olshausen 2001). The hierarchical model has also encouraged the search for coding principles that, when applied layer after layer in a hierarchy, will develop simple and complex-like behavior in a sequence (Hoyer and Hyvarinen 2002; Hyvarinen and Hoyer 2001; Rao and Ballard 1997, 1999).

Therefore we believe the discreteness of simple/complex cells is more than a technical discussion about how to define these classes of neurons; the concept has become an integral part of many theoretical and modeling approaches to cortical function. At stake is the wide belief that V1 cortex can be considered as composed of a hierarchy of distinct classes of receptive fields. The null hypothesis is that receptive fields lie along a continuum with simple and complex cells at the ends. If we accept the view that RF properties lie on a continuum, it would make sense to seek theoretical models that explain the *distribution* of receptive field properties *and their correlations* across the entire population, as well as trends in receptive field properties with laminar location (Ringach 2004). Such theories would have a quite different flavor than current ones that assume a "building-block" cortex with simple and complex cells organized in a strict hierarchy. Thus the discreteness of neural populations in the cortex is something we must consider seriously, as the outcome may have a strong impact on how one views cortical organization and function.

ACKNOWLEDGMENTS

We thank J. Dorn, B. Malone, and C. Bredfeldt for data collection and valuable comments and discussions. We thank J. Victor, S. Engel, F. Mechler, B. Shapley, M. Gur, A. Saul, M. Snodderly, and I. Kagan for feedback on an earlier version of this manuscript.

GRANTS

This research has been supported by National Eye Institute Grant EY-12816 and a Research to Prevent Blindness grant to the Jules Stein Eye Institute at UCLA.

REFERENCES

Abbott LF and Chance FS. Rethinking the taxonomy of visual neurons. *Nat Neurosci* 5: 391–392, 2002.

Bell AJ and Sejnowski TJ. The "independent components" of natural scenes are edge filters. *Vision Res* 37: 3327–3338, 1997.

Cai D, DeAngelis GC, and Freeman RD. Spatiotemporal receptive field organization in the lateral geniculate nucleus of cats and kittens. *J Neurophysiol* 78: 1045–1061, 1997.

Chance FS, Nelson SB, and Abbott LF. Complex cells as cortically amplified simple cells. *Nat Neurosci* 2: 277–282, 1999.

Conway BR and Livingstone MS. Space-time maps and two-bar interactions of different classes of direction-selective cells in macaque V-1. *J Neurophysiol* 89: 2726–2742, 2003.

De Valois KK, De Valois RL, and Yund EW. Responses of striate cortex cells to grating and checkerboard patterns. *J Physiol* 291: 483–505, 1979.

De Valois RL, Albrecht DG, and Thorell LG. Spatial frequency selectivity of cells in macaque visual cortex. *Vision Res* 22: 545–559, 1982.

Dean AF and Tolhurst DJ. On the distinctness of simple and complex cells in the visual cortex of the cat. *J Physiol* 344: 305–325, 1983.

DeAngelis GC, Ghose GM, Ohzawa I, and Freeman RD. Functional micro-organization of primary visual cortex: receptive field analysis of nearby neurons. *J Neurosci* 19: 4046–4064, 1999.

Ferster D. Spatially opponent excitation and inhibition in simple cells of the cat visual cortex. *J Neurosci* 8: 1172–1180, 1988.

Haralick RM and Shapiro LG. *Computer and Robot Vision.* Reading, MA: Addison-Wesley, vol. 1, 1992.

Heggelund P. Quantitative studies of the discharge field of single cells in cat striate cortex. *J Physiol* 373: 277–292, 1986a.

Heggelund P. Quantitative studies of enhancement and suppression zones in the receptive field of simple cells in cat striate cortex. *J Physiol* 373: 293–310, 1986b.

Henry GH. Receptive field classes of cells in the striate cortex of the cat. *Brain Res* 133: 1–28, 1977.

Hirsch JA. Synaptic physiology and receptive field structure in the early visual pathway of the cat. Cereb. Cortex 13: 1363–1369, 2003.

Hirsch JA, Martinez LM, Alonso JM, Desai K, Pillai C, and Pierre C. Synaptic physiology of the flow of information in the cat's visual cortex in vivo. *J Physiol* 540: 335–350, 2002.

Hoyer PO and Hyvarinen A. A multi-layer sparse coding network learns contour coding from natural images. *Vision Res* 42: 1593–1605, 2002.

Hubel DH and Wiesel TN. Receptive fields, binocular interaction and functional architecture in the cat's visual cortex. *J Physiol* 160: 106–154, 1962.

Hubel DH and Wiesel TN. Receptive fields and functional architecture of monkey striate cortex. *J Physiol* 195: 215–243, 1968.

Hurri J and Hyvarinen A. Simple-cell-like receptive fields maximize temporal coherence in natural video. *Neural Comput* 15: 663–691, 2003.

Hyvarinen A and Hoyer PO. A two-layer sparse coding model learns simple and complex cell receptive fields and topography from natural images. *Vision Res* 41: 2413–2423, 2001.

Jones JP and Palmer LA. The two-dimensional spatial structure of simple receptive fields in cat striate cortex. *J Neurophysiol* 58: 1187–1211, 1987.

Jones JP, Stepnoski A, and Palmer LA. The two-dimensional spectral structure of simple receptive fields in cat striate cortex. *J Neurophysiol* 58: 1212–1232, 1987.

Kagan I, Gur M, and Snodderly DM. Spatial organization of receptive fields in V1 neurons of alert monkeys: comparison with responses to gratings. *J Neurophysiol* 88: 2557–2574, 2003.

Kulikowski JJ and Bishop PO. Fourier analysis and spatial representation in the visual cortex. *Experientia* 37: 160–163, 1981.

Maffei L and Fiorentini A. The visual cortex as a spatial frequency analyser. *Vision Res* 13: 1255–1267, 1973.

Maske R, Yamane S, and Bishop PO. Simple and B-cells in cat striate cortex. Complementarity of responses to moving light and dark bars. *J Neurophysiol* 53: 670–685, 1985.

Mechler F and Ringach DL. On the classification of simple and complex cells. *Vision Res* 42: 1017–1033, 2002.

Movshon JA, Thompson ID, and Tolhurst DJ. Receptive field organization of complex cells in the cat's striate cortex. *J Physiol* 283: 79–99, 1978a.

Movshon JA, Thompson ID, and Tolhurst DJ. Spatial summation in the receptive fields of simple cells in the cat's striate cortex. *J Physiol* 283: 53–77, 1978b.

Olshausen BA. Sparse codes and spikes. In: *Probabilistic Models of the Brain: Perception and Neural Function,* edited by Rao RPN, Olshausen BA, and Lewicki MS. Cambridge, MA: MIT Press, 2001, p. 257–272.

Olshausen BA and Field DJ. Emergence of simple-cell receptive field properties by learning a sparse code for natural images. *Nature* 381: 607–609, 1996.

Palmer LA and Davis TL. Receptive-field structure in cat striate cortex. *J Neurophysiol* 46: 260–276, 1981.

Priebe N, Mechler F, Carandini M, and Ferster D. The contribution of the action potential threshold to the dichotomy between simple V1 simple and complex cells. *Nat Neurosci* 7: 1113–1122, 2004.

Rao RP and Ballard DH. Dynamic model of visual recognition predicts neural response properties in the visual cortex. *Neural Comput* 9: 721–63, 1997.

Rao RP and Ballard DH. Predictive coding in the visual cortex: a functional interpretation of some extra-classical receptive-field effects. *Nat Neurosci* 2: 79–87, 1999.

Ringach DL. Mapping receptive fields in visual cortex. *J Physiol* 558: 717–728, 2004.

Ringach DL, Bredfeldt CE, Shapley RM, and Hawken MJ. Suppression of neural responses to nonoptimal stimuli correlates with tuning selectivity in macaque V1. *J Neurophysiol* 87: 1018–1027, 2002a.

Ringach DL, Shapley RM, and Hawken MJ. Orientation selectivity in macaque v1: diversity and laminar dependence. *J Neurosci* 22: 5639–5651, 2002b.

Schiller PH, Finlay BL, and Volman SF. Quantitative studies of single-cell properties in monkey striate cortex. III. Spatial frequency. *J Neurophysiol* 39: 1334–1351, 1976a.

Schiller PH, Finlay BL, and Volman SF. Quantitative studies of single-cell properties in monkey striate cortex. II. Orientation specificity and ocular dominance. *J Neurophysiol* 39: 1320–1333, 1976b.

Schiller PH, Finlay BL, and Volman SF. Quantitative studies of single-cell properties in monkey striate cortex. I. Spatiotemporal organization of receptive fields. *J Neurophysiol* 39: 1288–1319, 1976c.

Simoncelli EP and Olshausen BA. Natural image statistics and neural representation. *Annu Rev Neurosci* 24: 1193–1216, 2001.

Simoncelli EP, Pillow J, Paninski L, and Schwartz O. Characterization of neural responses with stochastic stimuli. In: *The Cognitive Neurosciences,* edited by Gazzaniga, M. Cambridge MA: MIT Press, 2004, chapt. 23.

Skottun BC, De Valois RL, Grosof DH, Movshon JA, Albrecht DG, and Bonds AB. Classifying simple and complex cells on the basis of response modulation. *Vision Res* 31: 1079–1086, 1991.

Spitzer H and Hochstein S. A complex-cell receptive-field model. *J Neurophysiol* 53: 1266–1286, 1985a.

Spitzer H and Hochstein S. Simple- and complex-cell response dependences on stimulation parameters. *J Neurophysiol* 53: 1244–1265, 1985b.

Spitzer H and Hochstein S. Complex-cell receptive field models. *Prog Neurobiol* 31: 285–309, 1988.

Tao L, Shelley M, McLaughlin D, and Shapley R. An egalitarian network model for the emergence of simple and complex cells in visual cortex. *Proc Natl Acad Sci USA* 101: 366–371, 2004.